Research Article
https://doi.org/10.33904/ejfe.1516227
© Copyright 2025 by Forest Engineering and Technologies Platform on-line at https://dergipark.org.tr/en/pub/ejfe

Eur J Forest Eng 2025, 11(2):81-94

EJFE

Maple Species Identification Based On Hyperspectral Imaging Time Series

Pavel A. Dmitriev*, Boris L. Kozlovsky, Anastasiya A. Dmitrieva

Southern Federal University, Academy of Biology and Biotechnologies, 344006 Rostov-on-Don, Russia

Abstract

The aim of the study was to identify *Acer campestre* L., *A. negundo* L., and *A. saccharinum* L. from time-series hyperspectral data. Maple leaves were subjected to Hyperspectral Imaging (HSI) in laboratory conditions every 7-10 days for two years. Random forest (RF), correlation analysis, principal component analysis (PCA), PCA-RF and Gini index were used to determine significant spectral bands for species classification. This paper demonstrates that maple species can be accurately classified during specific periods of the growing season with a success rate exceeding 90%. These periods can vary from year to year. Research has demonstrated that using seven spectral bands is adequate for classifying maple species, while using twenty spectral bands can maximize accuracy. The repeatability of the obtained results confirms their representativeness over time and when using different methods of data processing.

Keywords: Spectral bands, Acer, Photosynthetic pigments, Remote sensing, Random forest.

1. Introduction

Monitoring woody vegetation is an important ecological, environmental, and social task. Forest vegetation usually occupies large areas. Their ground-based surveys are therefore very labour-intensive and insufficiently rapid. It is possible to assess the qualitative and quantitative characteristics of tree species within forest vegetation over large areas using unmanned aerial vehicles (UAVs) (Dainelli et al., 2021). In this direction, the main problem is the identification of tree species. This problem has been solved for grassy agricultural crops, which can be classified according to the vegetation indices (VIs) time-series (Heupel et al., 2018; Bozo et al., 2020; Saeed et al., 2021). Differences in the VIs time series for agricultural crops are associated with the specifics of their phenological cycles and agricultural technology. The problem of classifying trees in forests arises because they differ little in the phenological cycle, grow densely, and are diffusely located (Dadon et al., 2019).

Recently, the number of works devoted to attempts to identify tree species by remote sensing (RS) has been growing (Fassnacht et al., 2016; Dainelli et al., 2021). Various technologies and sensors have been used to identify tree species – RGB (Sivanandam et al., 2022; Veras et al., 2022; van Geffen et al., 2022), LiDARs and multispectral cameras (Guo et al., 2022; Norton et al., 2022; Lassalle et al., 2023). There is great interest in the capabilities of hyperspectral cameras (Miyoshi et al., 2020, 2020a; Gimenez et al., 2021; Tang et al., 2022), which provide more detailed spectral information about the object compared to multispectral sensors. Recent advances in RS, which have been increasingly used in forestry (Dainelli et al., 2021), have led the predominantly use of hyperspectral sensors to identify tree species with UAVs, and LiDARs are used to detect individual trees and their inventory. The increasing availability and advancements of hyperspectral cameras, along with the development of UAVs, have made their widespread use possible (Fassnacht et al., 2016). UAV can combine the advantage of high-resolution imagery with quick turnaround series, being therefore suitable for routine forest stand monitoring and real-time applications (Chianucci, 2016). At the same time, it should be emphasized that hyperspectral cameras, due to their complexity and high cost, remain a tool for theoretical and applied scientific research, including for the development of RS technologies.

Undoubtedly, the use of spectral characteristics in time-series studies throughout the entire vegetation period of a tree, can significantly improve classification accuracy. Typically, the assessment of tree plantings relies on time-series data of spectral characteristics collected over a single growing season, as a rule of thumb (Dash et al., 2018; Berra et al., 2019; Dmitriev et al., 2024). However, only a few studies extend their analysis to cover more than one growing season (Miyoshi et al., 2020b).

*Corresponding Author: Tel: +7 9604500405 E-mail: *pdmitriev@sfedu.ru*
Received: 14 July 2024; Accepted: 19 December 2024
This work is licensed under a Creative Commons Attribution-NonCommercial 4.0 International License

Many algorithms have been applied to the classification of the species, such as Random forest (RF), support vector machine (SVM) (Franklin et al., 2018; Norton et al., 2022; Guo et al., 2022), convolutional neural network (CNN) (Fricker et al., 2019; Sothe et al., 2020; Lassalle et al., 2023). RF is more proper because it requires fewer computational resources and much less training time. Also, RF provides quite high classification accuracy. Significant progress has been made in the identification of tree species. Nevertheless, classifying trees into specific species remains a challenge (Hycza et al., 2018; Iglhaut et al., 2019; Xu et al., 2020).

For our study, During the experiment, we assumed that the ability to identify specific tree species from Hyperspectral Imaging (HSI) data should be demonstrated under controlled laboratory conditions. The reliability of the results must be ensured by repeating the experiment during the growing season and over the years. The study by Rehman et al. (2022) showed that the importance of such studies for the development of RS technologies is increasing following the concurrence of results from aerial and proximal surveys. Three species of maple were chosen as objects of study. For the experiment, we have time-series of 125 spectral bands (SB) for two periods of maple vegetation (2021 and 2022). In this study, we used only SB for species classification and did not use VIs. First, it is important to determine the bands (or groups of bands) that are significant for the classifying species/ Once it is determined, we can search for or VIs. This approach is more suitable for addressing practical issues, such as the development of multispectral sensor. For classification, RF was chosen as the main classification method.

To achieve this goal, it was necessary to address the following tasks:

- Identify the period in the annual growth cycle of maples when species classification based on SB can be performed most accurately.
- Determine the SB (or spectrum intervals) provide the most valuable information for species classification;
- Determine groups of SB that are closely correlated with each other in terms of HSI and reduce the number of bands for classifying maples;
- Validate the results by repeating the experiment during different stages of the growing season and across multiple years.

2. Materials and Methods

2.1. Study Area and Data

The study was conducted at the Southern Federal University (Russia) in 2021 and 2022 (Figure 1). The study focused on three species of maple: *Acer campestre*, *A. negundo* and *A. saccharinum*. Each species was represented by three trees. All maple trees were grown under the same conditions. Ten leaves were taken from the crown of each tree. Leaves were transported for one hour to the laboratory where imaging was performed under artificial light using a Cubert UHD-185 hyperspectral camera (Aasen et al., 2015; Bareth et al., 2015; Dmitriev et al., 2023). The camera lens was located at 40 cm above the leaf blade and directed perpendicular to it (Figure 1). In this case, the pixel size was 25 cm x 25 cm.

In 2021, the study was conducted on: May 13, May 19, Jun 04, Jun 18, Jun 25, Jul 02, Jul 09, Jul 16, Jul 23, Aug 06, Aug 24, Aug 27, Sep 03, Sep 10, Sep 16, Sep 24, Oct 01, Oct 08. In 2022, the study was conducted on: May 06, May 13, May 19, May 27, Jun 03, Jun 10, Jun 16, Jun 27, Jul 04, Jul 18, Jul 25, Jul 29, Aug 09, Aug 15, Aug 30, Sep 05, Sep 12, Sep 20, Sep 27, Oct 03, Oct 10, Oct 17, Oct 24.

2.2. Method

To determine the content of photosynthetic pigments, the spectrophotometric method was used. The content of pigments was determined in the extract from acetone and recalculated per dm^2. Sampling for the determination of photosynthetic pigments in 2021 was carried out on the same calendar dates as the HSI. In 2022, photosynthetic pigments were determined on the following calendar dates: May 25, Jun 26, Jul 27, Aug 30, Sep 27.

Selecting the most informative spectral bands for species classification is crucial. Informative spectral bands can serve as valuable taxonomic traits. Additionally, reducing the number of spectral bands is essential for developing efficient and cost=effective multispectral sensors.

The SB were screened according to the following principles:

- Based on the results of principal component analysis (PCA)
- Exclusion of closely correlated SB,
- By the largest contribution to the value in th,e OOB estimate of error rate RF pixel-based classification by selecting their optimal combinations,
- Based on the results of PCA-RF pixel-based classification,
- Based on the Gini index.

One of the ways to solve the problem is to enumerate all possible combinations of SB and select the optimal combination, which gives the smallest OOB estimate of error rate. However, with our technical capabilities, this is not possible. Therefore, a simpler way was selection. At first, two SB were selected which, gave the lowest OOB estimate of error rate. The third SB was then selected, which, in combination with the first two, gave the smallest error. Next, the fourth SB was selected and the process was repeated. In this way, the entire available data set was analysed. To determine the optimal number of SB for RF pixel-based classification, we used the scree plot method (SPM) (Cattell, 1966). The SPM allows for finding the point (the number of SB) where the decrease in OOB estimate of error rate slows down the most.

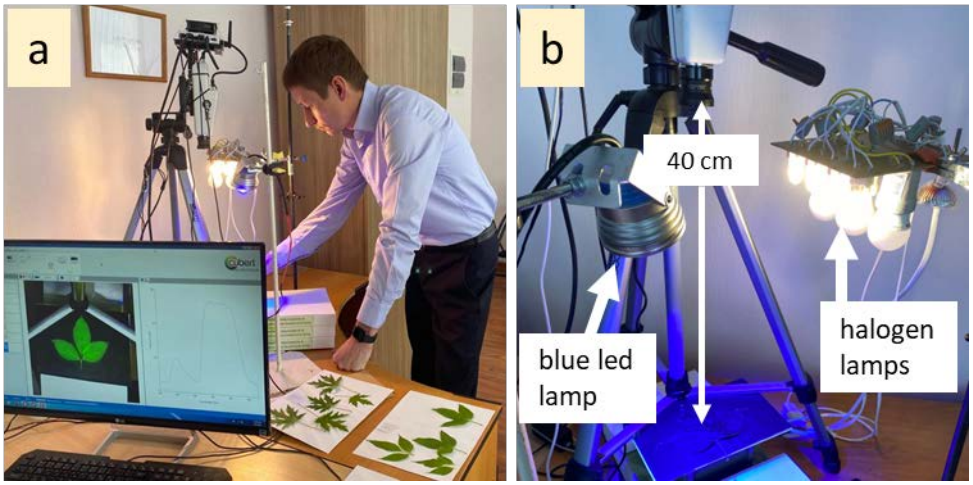


Figure 1. Conducting an experiment (a) and spectral collection equipment (b)

Using the PCA method, we aimed to identify the SB that provide are the most information for RF pixel-based classification. It can be assumed that the most informative SBs will exhibit high factors loadings on significant components. The PCA was conducted during the optimal timing of the growing season for maples, during which the RF classification error is relatively stable and the smallest.

Gini index is a statistical indicator of the degree of pixel stratification by the value of the SB. If the Gini value is equal to 0, then the pixels are evenly distributed over the values of the SB. The higher the Gini value, the more quartiles (groups) the set of pixels is stratified. The reason for this separation is that the pixels belong to different species of maple. Therefore, the higher the Gini value of the SB, the more interesting it is for the maple classification.

3. Results

3.1 Determination of the vegetation interval of maples, optimal for their identification

Based on the results of RF Pixel-based classification of maple leaves by species, the seasonal dynamics of Out-of-bag (OOB) estimate of error rate over two years was calculated (Figure 2). On the curves of the OOB estimate of error rate, it is possible to identify segments where the OOB estimate of error rate is relatively stable and not high (from 4 to 12%). For 2021, the interval is from Jun 18 to Aug 24, and for 2022, the interval is from Aug 09 to Oct 24. The periods for optimal classification of maples by the RF method differ by years and overlap only in august. At the beginning of the growing season, the OOB estimate of error rate is high in both years of the study (Figure 3).

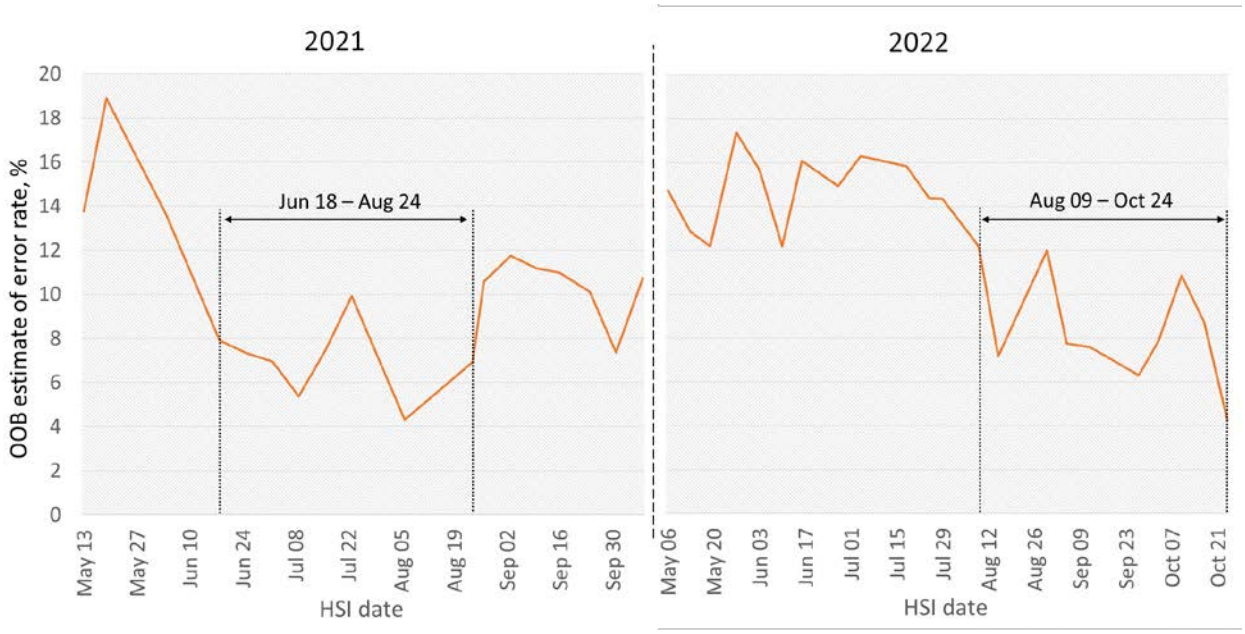


Figure 2. Seasonal dynamics of OOB estimate of error rate RF pixel-based classification of leaves *Acer campestre*, *A. negundo* and *A. saccharinum*

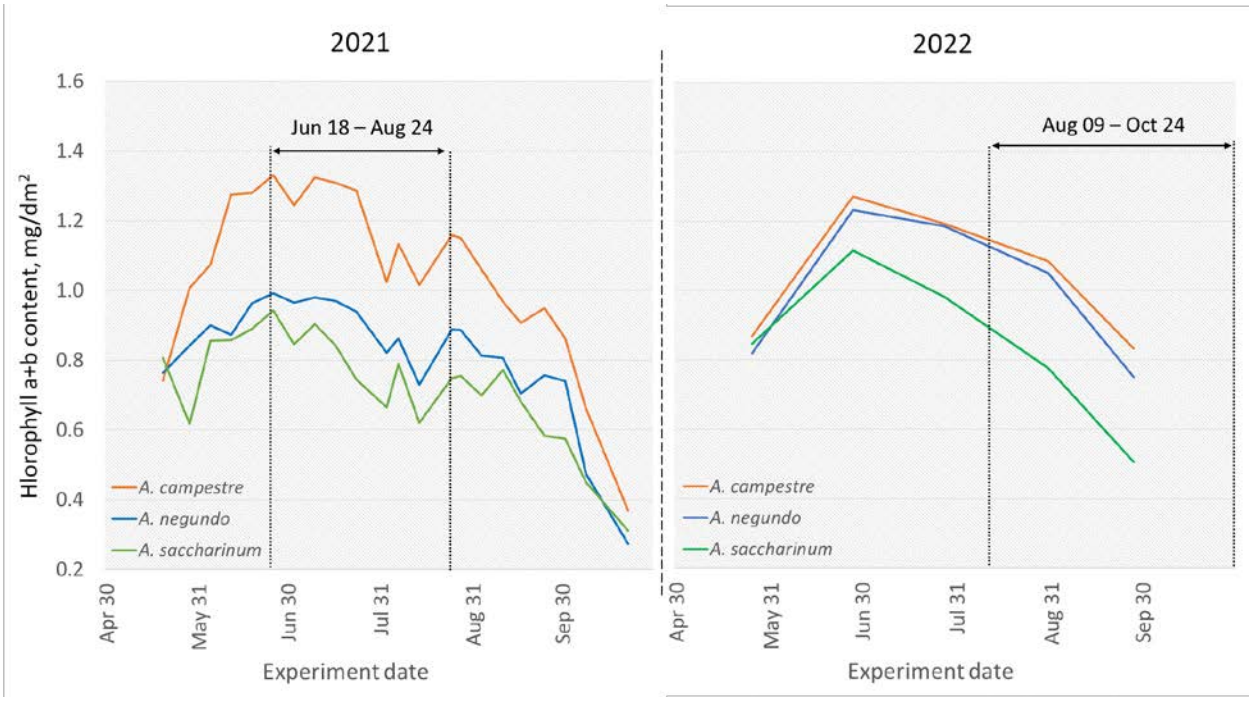


Figure 3. Seasonal dynamics of the content of the sum of chlorophylls *a* and *b* in maples in 2021 and 2022

3.2 Screening of the most informative spectral bands for maple species classification using Random Forest

3.2.1 Screening with PCA

When examining the results of the PCA from 2022, the variances of 125 SB corresponding to significant principal components is presented in Appendix A. The number of significant components (factors) in accordance with the Kaiser criterion for most calendar dates of HSI is 6, less often 7, and for one calendar date is 8. The cumulative proportion for the first two principal components (PCs) is in the range from 0.60 to 0.70. Factor loads of SB on significant components are low and do not exceed 0.375. It is may be due to data redundancy. Most SBs have insignificant (less than 0.2) loads on significant components that we did not consider. If we average the PCA results over all calendar dates of the HSI, then factor loadings of more than 0.2 are noted: on the 3rd and 4th PCs for the SB 454 - 490 nm; on 5 - 6 PCs for SB 648 - 686 nm; on 3 - 4 (5, 7) PCs for SB 930 - 950 nm. For four calendar dates of HSI, significant factor loadings are fixed on the 7th PCs for SB in the range from 502 to 520 nm (Appendix A). We believe that PCA results are not reliable due to low factor loadings. Therefore, other approaches were used to select informative SB.

3.2.2 Excluding closely correlated SB during screening

The availability of time series for SB allows calculation of the coefficient of determination (R^2) between their values and the calendar dates of HSI for each species of maple. The matrix of determination coefficient values is shown in Figure 4-6. The threshold for R^2 value was set at 0.9 or higher when selecting groups of correlating SB. It is characteristic that the matrix of values of the coefficient of determination is the same for all three species, this pattern is repeated over the years. As can be seen in Figure 4-6, SB that are closely correlated with each other in terms of values form seven groups.

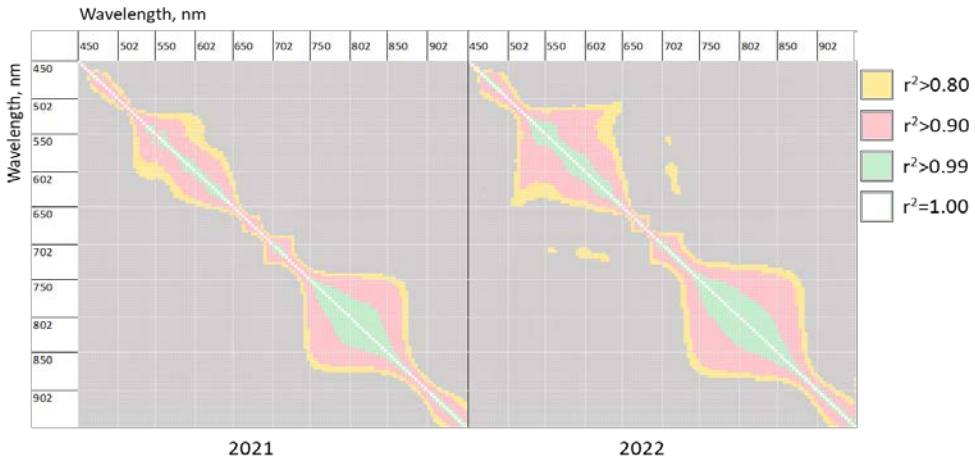


Figure 4. Matrix of values of the coefficient of determination between SBs for *A. campestre*

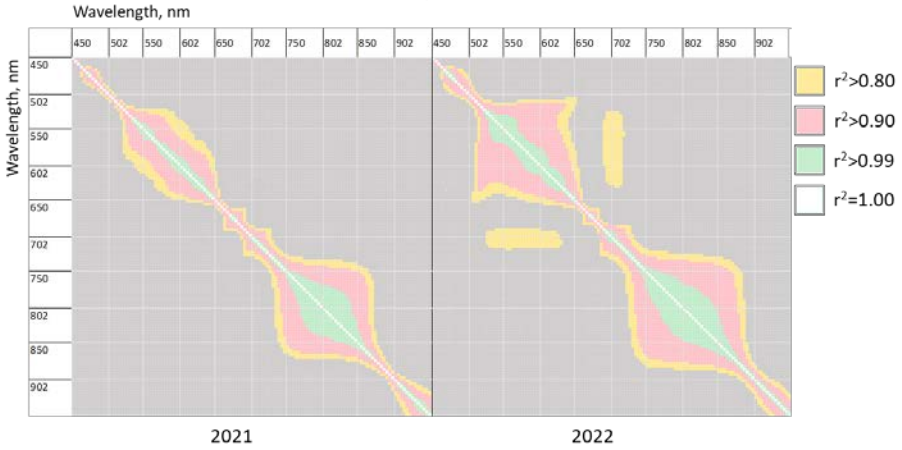


Figure 5. Matrix of values of the coefficient of determination between SBs for *A. negundo*

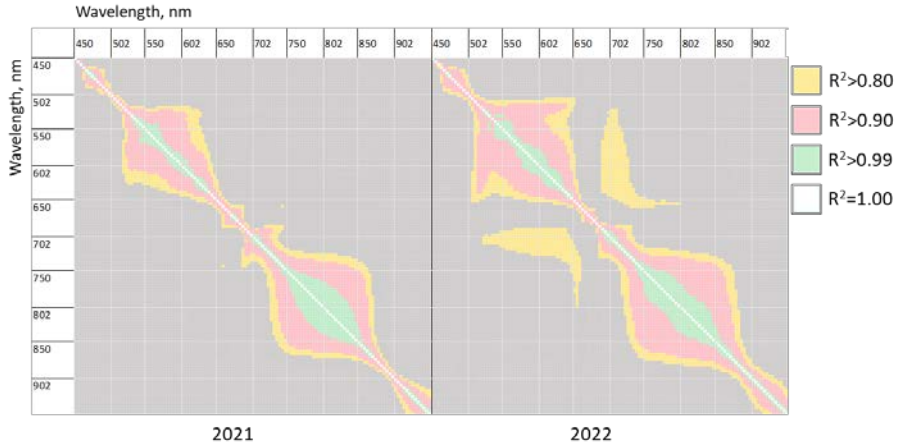


Figure 6. Matrix of values of the coefficient of determination between SBs for *A. saccharinum*

The wavelengths are organizedin ascending order within the following spectral ranges: 462 to 486 nm, 522 to 598 nm, 598 to 650 nm, 662 to 690 nm, 690 to 730 nm, 730 to 870 nm, and 902 to 946 nm. The groups have different sizes, while they combine 80% of the SB and cover the entire spectral range of Cubert UHD-185. In this regard, it is necessary to analyze the seasonal dynamics of the values of the SB within the correlating groups, as well as to compare them between the groups. For this, graphs of the seasonal dynamics of 125 SB for 2021 and 2022 of the experiment were plotted (Figure 7).

The main conclusions drawn from the analysing the seasonal dynamics of the SB are as follows:

- The nature of the seasonal dynamics of the SB changes when moving from one correlating group to another. Linear dependence changes to parabolic and vice versa.
- The greatest difference between maple species in terms of SB values was noted in the first (462 - 486 nm), second (522 - 598 nm), and fourth groups (662 - 690 nm).
- The general nature of the seasonal dynamics of the values of the SB of maples is repeated over the years (except a group of SBs in the range of 902 - 946 nm). The location of the regression lines for the values of the SB of maple species relative to each other is also repeated over the years.
- The results suggested that the number of SB needed to characterize maples can be reduced. It should be noted that while correlation analysis helps decrease the number of spectral bands for classifying maples, it does not enable us to identify which bands are the most informative for pixel-based classification using random forest (RF) methods. The regression lines for different maple species are qualitatively similar. In most cases, they are completely identical in form and trends and differ only in SB values (Figure 7). Therefore, they cannot be used as original spectral signatures for species identification.

3.2.3 Screening of SB by selecting their optimal combinations by RF OOB estimate of error rate

Each SB was then ranked according to its contribution to the OOB estimate of error rate. SPM graphs reflecting the dependence of the OOB estimate of error rate on the number of SBs used in the RF matrix are shown in Figures 8 and 9. Based on the analysis of the SPM graphs, which relate the OOB estimate of error rate values to the number of SB in the RF matrix, the following conclusions are drawn:

- When using the optimal combination of seven to ten SB, the decrease in the OOB estimate of error rate occurs linearly.
- The point where the decrease in OOB estimate of error rate slows down the most is at 20 SB.
- With an increase in the number of SB, there is a slight increase in the OOB estimate of error rate, which can be explained by the Hughes phenomenon. In our case, an excessive number of SBs not only complicates the calculations but also reduces accuracy of the result.

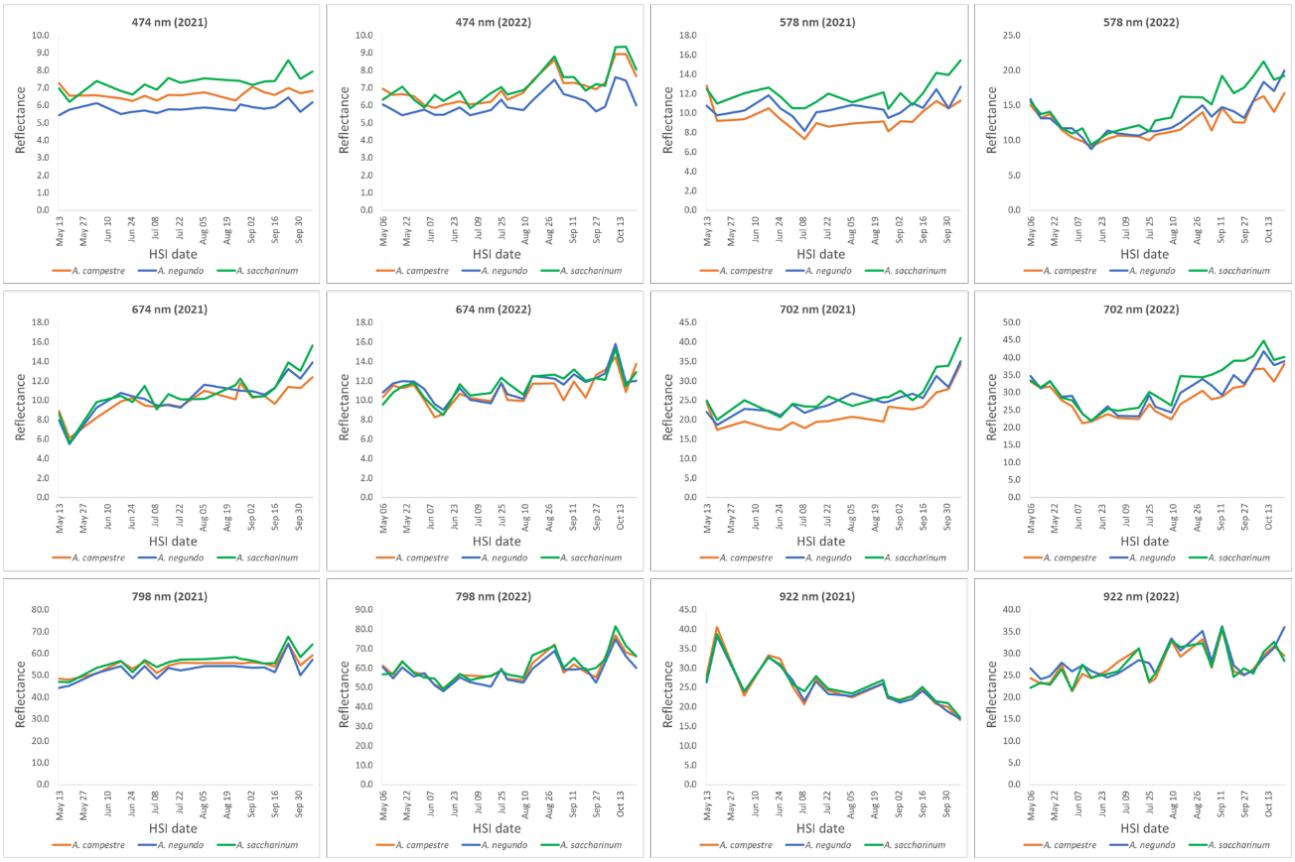


Figure 7. Empirical regressions of seasonal dynamics of SB by correlated groups

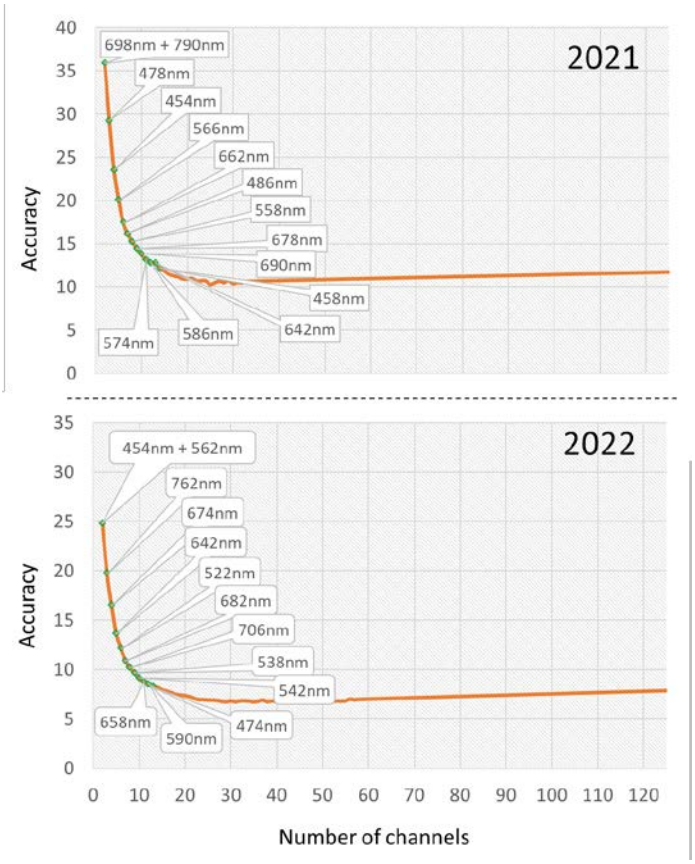


Figure 8. SPM graphs of OOB estimate of error rate depending on the number of SB (Calendar dates: 2021.10.09; 2022.10.03)

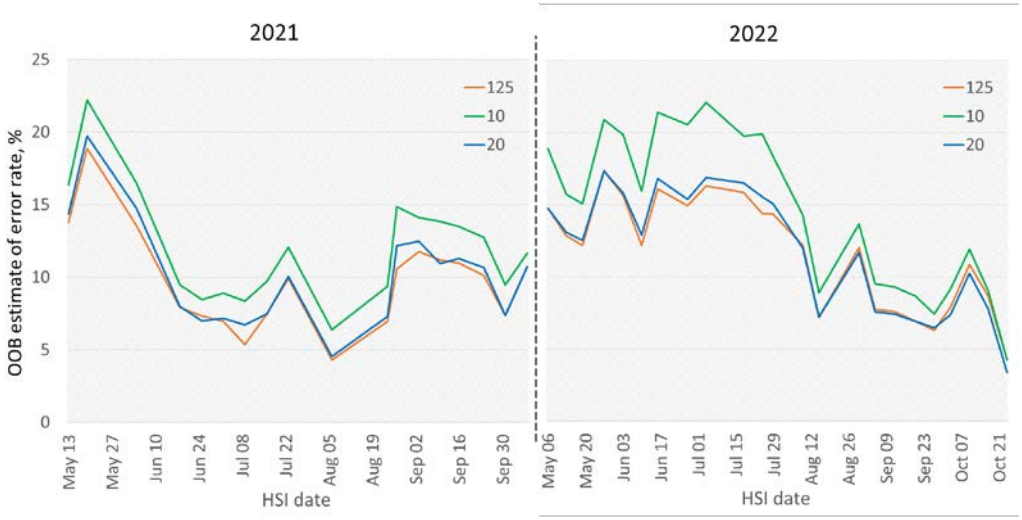


Figure 9. Dynamics of OOB estimate of error rate RF pixel-based classification of leaves of three species of *Acer campestre*, *A. negundo* and *A. saccharinum* according to the values of 10, 20 and 125 SB

These patterns of SPM graphs across calendar dates throughout the season and weather persist. The seasonal dynamics of the OOB estimate of error rate depending on the number of SB are shown in Figure 9. It is clearly seen that to obtain the lowest possible OOB estimate of error rate in the RF matrix, 20 SB are sufficient. The results of using 10 SB are also satisfactory for certain segments of the maple seasonal cycle.

To determine the SB that contributes most to error reduction, ranks were assigned to each of the first 20 SB based on the SPM results (Figure 8) for all HIS calendar dates. The first two SB were ranked 19.5, and the twentieth SB was ranked 1. The rank sum obtained for each SB was divided by the number of HSIs made during the season (Figure 10). Significant SB identified by RF pixel-based classification are located in the ranges of 450-494, 530-570, 590-610, 650-706, and 910-950 nm. The selected ranges by year match well.

3.2.4 Selection of SB significant for maple identification by PCA-RF pixel-based classification

An analysis of the data array of SB was carried out using the PCA-RF pixel-based classification method (Xu et al., 2021). To analyze the results obtained, SPM graphs were constructed by reflecting the dynamics of the OOB estimate of error rate RF pixel-based classification values depending on the number of PCs (Figure 11). The value of the OOB estimate of error rate RF pixel-based classification decreases sharply and reaches its minimum at the seventh PC – this is the point where the decrease in OOB estimate of error rate slows down the most. This is logical, since PCA analysis from the values of the SB showed that there are seven significant PCs (Section 3.2.1). Further, with an increase in the number of OOB components, the estimate of error rate begins to grow.

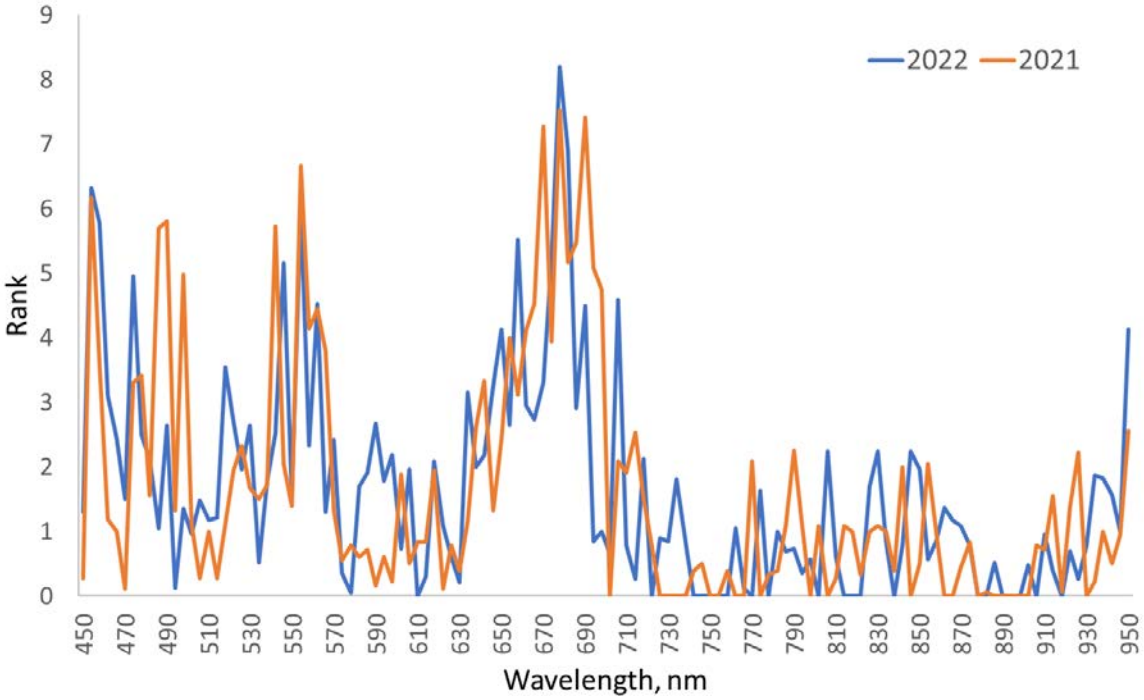


Figure 10. The average value of the rank of the contribution of SB to the OOB estimate of error rate

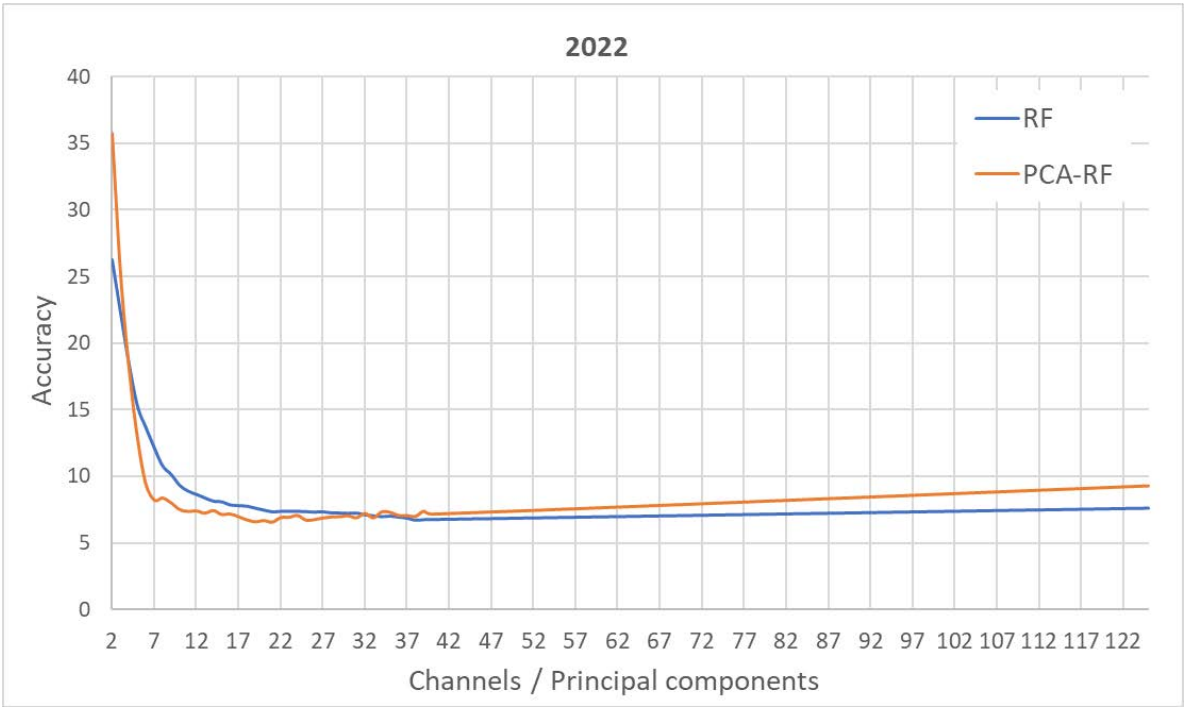


Figure 11. Dependence of OOB estimate of error rate on the number of main PCs and SB

When we compare the classification accuracy of RF pixel-based classification and PCA-RF pixel-based classification, the latter method, in most cases increases the classification accuracy by several percent at a point corresponding to seven PCs and seven SB (Figure 11).

After this point, the OOB estimate of error rate for the PCA-RF pixel-based classification method begins to increase and becomes higher than that of RF pixel-based classification. PCA-RF pixel-based classification shows that the significant SB for identifying maple species are associated with the first seven PCs.

3.2.5 Selection of SB significant for maple identification using Gini index

The Gini index values for SB averaged over the 2022 HSI calendar dates are shown in Figure 12. The results obtained using the Gini index align well with the results presented in Section 3.2.3. The peaks of the Gini index values occur in the intervals from 450 to 500, from 530 to 610, from 670 to 710 nm, and from 890 to 930 nm. The interval from 710 to 890 nm is of no interest for the classification of maples.

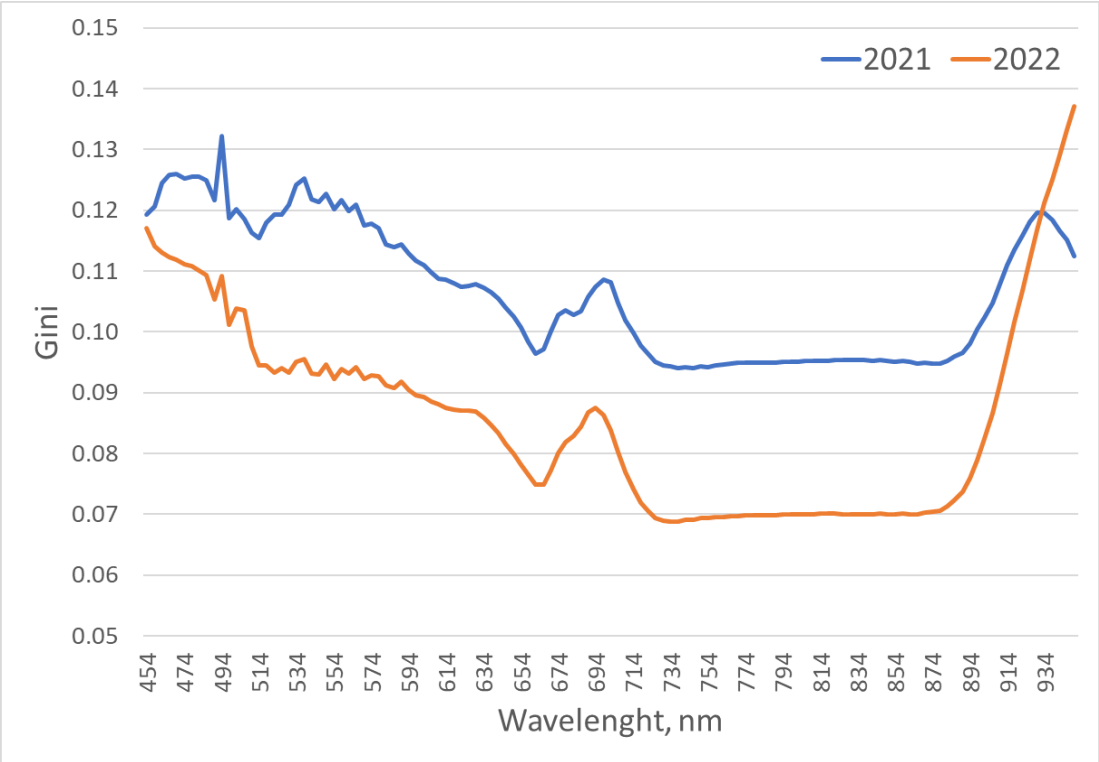


Figure 12. Averaged over the calendar dates of the HSI, the values of the Gini index by SB

4. Discussion

To determine which ranges of the electromagnetic spectrum provide the most informative data for the RF classification of maple species, based on the results of different data processing methods, these are the ranges of 454 to 494 nm (blue and cyan), from 530 to 570 nm (green), from 590 to 610 nm (orange), from 650 to 706 nm (red) and from 910 to 950 nm (near infrared). The presence of seven closely correlated groups of SBs, covering about 80% of the Cubert UHD-185 spectral range, allows for reducing each selected spectrum range to a single SB when conducting detailed studies. Regarding these results, it can be observed that multispectral sensors have long used broadband channels in the NIR band along with several R, G, B bands (Colomina et al., 2014). For example, the SEQUOIA+ universal camera performs multispectral imaging in four SB – green (550 nm), red (660 nm), "red slope" channel (Red Edge, 735 nm), and near infrared (790 nm) (www.parrot.com). On the other hand, the study showed the great importance of the blue (440 - 485 nm) and orange (590 - 625 nm) range of the electromagnetic radiation spectrum for the classification of maples. We have analyzed formulas for calculating 80 VIs. It turned out that in the calculation of only three of them, the spectra of the blue zone are used. These are EVI (Huete et al., 1997) – 475 nm, PSND (Blackburn 1998) – 470 nm and TGI (Hunt et al., 2013) – 480 nm. In addition, the results of our study indicate that the informative SB of the blue zone is closer to the left edge in the range of 454 - 460 nm. The SB of the orange range of the electromagnetic spectrum is used only when calculating one VI, out of the considered 80 VIs. This is Carter3 (Carter, 1994) (605 nm). Another important question to address is whether the untransformed values of the SB can be utilized for high-precision and time-reliable identification of trees. Several studies have shown that using untransformed SB values for classifying plant species has yielded satisfactory results (Franklin et al., 2018; Li et al., 2022; Liu, 2022).

The results of our research provide a negative answer to this question. Thus, a satisfactory accuracy of RF classification (≥90%) is achieved only in certain segments of the maple vegetation period. The SB optimal for RF classification varies within the allocated spectrum zones depending on the date of the HSI and the year of the study. Additional studies are required to elucidate the reasons for the large variability of the OOB estimate of error rate over the years. However, as a hypothesis, it can be assumed that this is due to the seasonal dynamics of chlorophyll content, which can fluctuate over the years depending on the weather. The largest difference in the sum of chlorophylls a and b content simultaneously between the three maple species in 2021 and 2022 (Ignatova et al., 2024) corresponds to the optimal periods for RF classification (Figure 3).

It is important to note that the SB are not suitable for constructing original time series that could identify maple species. Differences in the seasonal dynamics of the SB values are only quantitative; the nature of the SB value curves is absolutely identical (Figure 7). Therefore, it is recommended to utilize the results of HSI for identifying tree species in a transformed format, such as using spectral indices. Currently, significant success has been achieved in species identification through the use of VIs. (Yang et al., 2019; Zhou et al., 2022; Zhong et al., 2022).

It should be noted that various VIs have been developed to assess photosynthetic activity, including the Normalized Difference Vegetation Index (NDVI) by Tucker (1979), the Soil-Adjusted Vegetation Index (SAVI) by Huete (1988), and the Enhanced Vegetation Index (EVI) by Huete et al. (1997), and the Simple Ratio (SR) by Jordan (1969). On the other hand, water content also have been Normalized Difference Water Index (NDWI) , Moisture Stress Index (MSI), Normalized Difference Infrared Index (NDII), nitrogen (NDNI) (Quemada et al., 2021), carbon (NDLI, CAI) stress MSI, GLI, SGI, PRI (Gamon et al., 1992), PSRI (Merzlyak et al., 1999), soil characteristics SARVI, TSAVI, SAVI (Huete, 1988) have been determined using VIs.

Recent studies have introduced original spectral indices for real-time identification of plant species (Ahmed et al., 2021; Zhou et al., 2022). The results obtained in our study are the first step in creating variants of such indices.

The main task of further research is to improve the accuracy of the classification of trees, regardless of the timing of the survey during the growing season and the year of the study. The main directions for improving the classification accuracy can be:

- Increasing the frequency of HSI to can provide more detailed time series that covers the entire vegetation growing season. Research has shown that the value of information for species classification improves as the number of HSI increases (Dash et al., 2018; Berra et al., 2019; Miyoshi et al., 2020). Additionally, combining data from different seasons yields positive results in enhancing the accuracy of tree classification. (Fang et al., 2018; Liu, 2022; Veras et al., 2022);
- The use of combined SB and VIs;
- Zooming in on a classification object – moving from a pixel to a superpixel, individual leaf, or canopy. It has been shown that the object-based approach outperforms the pixel-based approach (Jones et al., 2010; Myint et al., 2011; Kavzoglu et al., 2018);
- Combining spectral characteristics (SB and VIs) with morphometric features of plants. This is confirmed by good results of tree identification based on combined data from spectral sensors and LiDARS (Liu et al., 2017; Fang et al., 2018; Shi et al., 2018).

RF is the primary classification method used due to its effectiveness. It performs well with both parametric and non-parametric data, provides strong protection against overfitting, and demonstrates high efficiency. As a result, it is commonly utilized in remote sensing (RS) and various other fields (Georganos et al., 2019; Collin et al., 2020; Su et al., 2021).

5. Conclusion

Based on the studies *Acer campestre*, *A. negundo*, and *A. saccharinum*, the following patterns have been identified. Maple species can be classified using the RF pixel-based method, achieving a satisfactory OOB error rate of less than 10% during specific segments of the trees' growing season. However, the optimal time periods for classification may differ from year to year. The key factor in estimating the OOB error rate is the optimal combination of 7 to SBs. The highest classification accuracy is reached using 20 optimal SB. According to the results of selecting the optimal combination of SB for RF pixel-based classification, the most informative bands are those located in the ranges from 450 to 494, from 530 to 570, from 590 to 610, from 650 to 706 nm, and from 910 to 950 nm. A similar result was obtained from the Gini index, and the PCA method. Indirectly, the result confirms the PCA-RF pixel-based classification method, in which the maximum accuracy is achieved using the values of the seven PCs. Using correlation analysis, seven groups of SB with a strong correlation were found. They are arranged in ascending order in the following spectral ranges: 462 to 486 nm, 522 to 598 nm, 598 to 650 nm, 662 to 690 nm, 690 to 730 nm, 730 to 870 nm, and 902 to 946 nm. Comparing the results of RF pixel-based classification, PCA-RF pixel-based classification, and the use of the Gini index with the results of correlation analysis, we can assume that seven SB are sufficient for maple classification. Since the maximum possible accuracy is calculated in the study, and with the optimal number and combination of bands, this accuracy not sufficient for many calendar dates; it is necessary to convert the SB into VIs. This is confirmed to a certain extent by the PCA-RF pixel-based classification. The consistency of the results is validated by their repeatability across calendar dates and years of HSI, employing various data processing methods.

Ethics Committee Approval: N/A.

Peer-review: Externally peer-reviewed.

Author Contributions: Concept: P.A.D., B.L.K; Design: P.A.D.; Supervision: A.A.D.; Resources: P.A.D., B.L.K, A.A.D.; Data Collection: P.A.D., A.A.D.; Analysis: P.A.D., B.L.K.; Literature Search: B.L.K.; Writing Manuscript: P.A.D., B.L.K., A.A.D.; Critical Review: P. A.D., B.L.K.

Conflict of Interest: The authors have no conflicts of interest to declare.

Financial Disclosure: The project was supported by the Russian Science Foundation under grant No. 24-24-00405, https://rscf.ru/project/24-24-00405/, and performed in Southern Federal University (Rostov-on-Don, Russian Federation).

Cite this paper as: Dmitriev, P.A., Kozlovsky, B.L., Dmitrieva, A.A. 2025. Maple Species Identification Based On Hyperspectral Imaging Time Series, *European Journal of Forest Engineering*, 11(2): 81-94.

References

Al-Dahoud, A., Fezari, M., Alkhatib, A.A., Soltani, M. N., Al- Dahoud, A. 2023. Forest fire detection system based on low-cost wireless sensor network and internet of things. *WSEAS Transactions on Environment and Developmen*t, 19:506-513.

Aasen, H., Burkart, A., Bolten, A., Bareth, G. 2015. Generating 3D hyperspectral information with lightweight UAV snapshot cameras for vegetation monitoring: From camera calibration to quality assurance. *JPRS*, 108:245-259. https://doi.org/ 10.1016/j.isprsjprs.2015.08.002

Ahmed, S., Nicholson, C.E., Muto, P., Perry, J.J., Dean, J.R. 2021. Applied aerial spectroscopy: A case study on remote sensing of an ancient and semi-natural woodland. *PLoS ONE*, 16(11):e0260056. https://doi.org/10.1371/journal.pone.0260056

Bareth, G., Aasen, H., Bendig, J., et al. 2015. Low-weight and UAV-based hyperspectral full-frame cameras for monitoring crops: Spectral comparison with portable spectroradiometer measurements. *Photogramm Fernerkundung Geoinf,* 69-79. https://doi.org/ 10.1127/PFG/2015/0256

Berra, E.F., Gaulton, R., Barr, S. 2019. Assessing spring phenology of a temperate woodland: A multiscale comparison of ground, unmanned aerial vehicle and Landsat satellite observations. *Remote Sensing of Environment,* 223:229-242. https://doi.org/10.1016/ j.rse.2019.01.010

Blackburn, G.A. 1998. Quantifying chlorophylls and caroteniods at leaf and canopy scales: An evaluation of some hyperspectral approaches. *Remote Sens of Environ,* 66(3):273–285. https://doi.org/10.1016/ S0034- 4257(98)00059-5

Bozo, M., Aptoula, E., Çataltepe, Z. 2020. A Discriminative Long Short Term Memory Network with Metric Learning Applied to Multispectral Time Series Classification. *J Imaging,* 6:68. https://doi.org/ 10.3390/jimaging6070068

Carter, G.A. 1994. Ratios of leaf reflectances in narrow wavebands as indicators of plant stress. *Int J of Remote Sens,* 15(3):697–703. https://doi.org/10. 1080/01431169408954109

Cattell, R.B. 1966. The Scree test for the number of factors. *Multivariate Behavioral Research,* 1:245–276. http://dx.doi.org/10.1207/s15327906mbr0102 _10

Chianucci, F., Disperati, L., Guzzi, D., et al. 2016. Estimation of canopy attributes in beech forests using true colour digital images from a small fixed-wing UAV. *International Journal of Applied Earth Observation and Geoinformation,* 47:60-68. https://doi.org/10.1016/j.jag.2015.12.005

Collin, F.D., Durif, G., Raynal, L., et al. 2020. Extending Approximate Bayesian Computation with Supervised Machine Learning to infer demographic history from genetic polymorphisms using DIYABC Random Forest. *Molecular Ecology Resources*, 21(8): 2598-2613. https://doi.org/10.1111/1755-0998.13413

Colomina, I., Molina, P. 2014. Unmanned aerial systems for photogrammetry and remote sensing: A review. I*SPRS Journal of Photogrammetry and Remote Sensing*, 92:79-97. https://doi.org/10.1016/j.isprsjprs.2014.02.013

Dadon, A., Mandelmilch, M., Ben-Dor, E., Sheffer, E. 2019. Sequential PCA-based Classification of Mediterranean Forest Plants using Airborne Hyperspectral Remote Sensing. *Remote Sens*, 11:2800. https://doi.org/10.3390/rs11232800

Dainelli, R., Toscano, P., Di Gennaro, S.F., Matese, A. 2021 Recent Advances in Unmanned Aerial Vehicle Forest Remote Sensing—A Systematic Review. Part I: A General Framework. *Forests*, 12:327. https://doi.org/10.3390/f12030327

Dash, J.P., Pearse, G.D., Watt, M.S. 2018. UAV Multispectral Imagery Can Complement Satellite Data for Monitoring Forest Health. *Remote Sens*, 10:1216. https://doi.org/10.3390/rs10081216

Dmitriev, P.A., Kozlovsky, B.L., Dmitrieva, A.A., Varduni, T.V. 2023. Maple species identification based on leaf hyperspectral imaging data. Remote Sensing Applications: *Society and Environment*, 30:2352-9385. https://doi.org/10.1016/j.rsase.2023.100964

Dmitriev, P., Kozlovsky, B., Dmitrieva, A., Varduni, T. 2024. Identification of the Leaves of Ulmus pumila L., Tilia cordata Mill. and Acer campestre L. Using Vegetation Indices. *European Journal of Forest Engineering*, 10(1), 54-66. https://doi.org/10.33904/ejfe.1430606

Fang, F., McNeil, B.E., Warner, T.A., Maxwell, A.E. 2018. Combining high spatial resolution multi-temporal satellite data with leaf-on LiDAR to enhance tree species discrimination at the crown level. *International Journal of Remote Sensing*, 39:23. https://doi.org/10.1080/01431161.2018.1504343

Fassnacht, F.E., Latifi, H., Stereńczak, K., Lefsky, M. 2016. Review of studies on tree species classification from remotely sensed data. *Remote Sens Environ*, 186:64–87.

Franklin, S.E., Ahmed, O.S. 2018. Deciduous tree species classification using object-based analysis and machine learning with unmanned aerial vehicle multispectral data. *Int J Remote Sens*, 39:5236–5245. https://doi.org/10.1080/01431161.2017.1363442

Fricker, G.A., Ventura, J.D., Wolf, J.A., North, M.P., Davis, F.W., Franklin, J. 2019. A Convolutional Neural Network Classifier Iden- tifies Tree Species in Mixed-Conifer Forest from Hyperspectral Imagery. *Remote Sens*, 11(19):2326. https://doi.org/10.3390/rs11192326

Gamon, J.A., Peñuelas, J., Field, C.B. 1992. A narrow-waveband spectral index that tracks diurnal changes in photosynthetic efficiency. *Remote Sens of Environ*, 41(1):35–44. https://doi.org/10.1016/0034-4257(92)90059-S

Georganos, S., Grippa, T., Gadiaga, A.N., et al. 2019. Geographical random forests: a spatial extension of the random forest algorithm to address spatial heterogeneity in remote sensing and population modelling. *Geocarto International*, 36:2. https://doi.org/10.1080/10106049.2019.1595177

Gimenez, R., Lassalle, G., Hédacq, R., et al 2021. Exploitation of spectral and temporal information for mapping plant species in a former industrial site. *Int Arch Photogramm Remote Sens Spatial Inf Sci*, 559–566. https://doi.org/10.5194/isprs-archives-XLIII-B3-2021-559-2021

Guo, Q., Zhang, J., Guo, S., Ye, Z., Deng, H., Hou, X., Zhang, H. 2022. Urban Tree Classification Based on Object-Oriented Approach and Random Forest Algorithm Using Unmanned Aerial Vehicle (UAV) Multispectral Imagery. *Remote Sens*, 14:3885. https://doi.org/10.3390/rs14163885

Heupel, K., Spengler, D., Itzerott, S. 2018. A Progressive Crop-Type Classification Using Multitemporal Remote Sensing Data and Phenological Information. *PFG*, 86:53–69. https://doi.org/10.1007/s41064-018-0050-7

Huete, A. 1988. A soil-adjusted vegetation index (SAVI). *Remote Sens of Environ*, 25:295–309. https://doi.org/10.1016/0034-4257(88)90106-X

Huete, A.R., Liu, H.Q., Batchily, K., van Leeuwen, W. 1997. A comparison of vegetation indices over a global set of TM images for EOS–MODIS. *Remote Sens of Environ*, 59:440–451. https://doi.org/10.1016/S0034-4257(96)00112-5

Hunt, E.R., Doraiswamy, P.C., McMurtrey, J.E., et al. 2013. A visible band index for remote sensing leaf chlorophyll content at the canopy scale. *Int J of Appl Earth Observation and Geoinformation*, 21:103–112. https://doi.org/10.1016/j.jag.2012.07.020

Hycza, T., Stereńczak, K., Bałazy, R. 2018. Potential use of hyperspectral data to classify forest tree species. *N Z j of For Sci*, 48:18. https://doi.org/10.1186/s40490-018-0123-9

Iglhaut, J., Cabo, C., Puliti, S., et al. 2019. Structure from Motion Photogrammetry in Forestry: a Review. *Curr Forestry Rep*, 5:155–168. https://doi.org/10.1007/s40725-019-00094-3

Ignatova, M.A., Kozlovsky, B.L., Dmitrieva, A.A., Varduni, T.V., Dmitriev, P.A. 2024. Assessment of seasonal dynamics of photosynthetic pigments in maple leaves using vegetation indices calculated from hyperspectral imaging data. *AgroEcoInfo: Electronic scientific and production journal*, https://doi.org/10.51419/202142206

Jones, T.G., Coops, N.C., Sharma, T. 2010. Assessing the utility of airborne hyperspectral and LiDAR data for species distribution mapping in the coastal Pacific

Northwest, Canada. *Remote Sensing of Environment,* 114:2841-2852. https://doi.org/10.1016/J.RSE.2010.07.002

Jordan, C.F. 1969. Derivation of leaf-area index from quality of light on forest floor. *Ecol,* 50(4):663–678. https://doi.org/10.2307/1936256

Kavzoglu, T., Tonbul, H., Yildiz Erdemir, M., et al. 2018. Dimensionality Reduction and Classification of Hyperspectral Images Using Object-Based Image Analysis. *J Indian Soc Remote Sens,* 46:1297–1306. https://doi.org/10.1007/s12524-018-0803-1

Lassalle, G., Ferreira, M.P., Cué La Rosa L.E., et al. 2023 Advances in multi- and hyperspectral remote sensing of mangrove species: A synthesis and study case on airborne and multisource spaceborne imagery. *ISPRS Journal of Photogrammetry and Remote Sensing*, 195:298-312. https://doi.org/10.1016/j.isprsjprs.2022.12.003

Li, Y., Chai, G., Wang, Y., Lei, L., Zhang, X. 2022. ACE R-CNN: An Attention Complementary and Edge Detection-Based Instance Segmentation Algorithm for Individual Tree Species Identification Using UAV RGB Images and LiDAR Data. *Remote Sens*, 14:3035. https://doi.org/10.3390/rs14133035

Liu, H. 2022. Classification of urban tree species using multi-features derived from four-season RedEdge-MX data. *Computers and Electronics in Agriculture*, 194:106794. https://doi.org/10.1016/j.compag.2022.106794

Liu, L., Coops, N.C., Aven, N.W., Pang, Y. 2017. Mapping urban tree species using integrated airborne hyperspectral and LiDAR remote sensing data. *Remote Sensing of Environment,* 200:170-182. https://doi.org/10.1016/j.rse.2017.08.010

Merzlyak, M.N., Gitelson, A.A., Chivkunova, O.B., Rakitin, V.Y.U. 1999. Non-destructive optical detection of pigment changes during leaf senescence and fruit ripening. *Physiol Plant,* 106(1):135–141. https://doi.org/10.1034/J.1399-3054.1999.106119.X

Miyoshi, G.T., Arruda, Md.S., Osco, L.P., et al. 2020. A novel deep learning method to identify single tree species in UAV-based hyperspectral images. *Remote Sensing,* 12(8):1294. https://doi.org/10.3390/rs12081294

Miyoshi, G.T., Imai, N.N., Tommaselli, A.M.G., Honkavaara, E. 2020a. Spectral differences of tree species belonging to atlantic forest obtained from UAV hyperspectral images. *Int Arch Photogramm Remote Sens Spatial Inf Sci,* 49–54. https://doi.org/10.5194/isprs-archives-XLII-3-W12-2020-49-2020

Miyoshi, T.G., Imai, N.N., Garcia Tommaselli, A.M., Antunes de Moraes, M.V., Honkavaara, E. 2020b. Evaluation of Hyperspectral Multitemporal Information to Improve Tree Species Identification in the Highly Diverse Atlantic Forest. *Remote Sens*, 12(2):244. https://doi.org/10.3390/rs12020244

Myint, S.W., Gober, P., Brazel, A., Grossman-Clarke, S., Weng, Q. 2011. Per-pixel vs. object-based classification of urban land cover extraction using high spatial resolution imagery. *Remote Sensing of Environment,* 115:1145-1161. https://doi.org/10.1016/j.rse.2010.12.017

Norton, C.L., Hartfield, K., Collins, C.D.H., van Leeuwen, W.J.D., Metz, L.J. 2022. Multi-Temporal LiDAR and Hyperspectral Data Fusion for Classification of Semi-Arid Woody Cover Species. *Remote Sens,* 14:2896. https://doi.org/10.3390/rs14122896

Quemada, C., Pérez-Escudero, J.M., Gonzalo, R., Ederra, I., Santesteban, L.G., Torres, N., Iriarte, J.C. 2021. Remote Sensing for Plant Water Content Monitoring: A Review. *Remote Sens.* 13, 2088. https://doi.org/10.3390/rs13112088

Rehman, T.H., Lundy, M.E., Linquist, B.A. 2022. Comparative Sensitivity of Vegetation Indices Measured via Proximal and Aerial Sensors for Assessing N Status and Predicting Grain Yield in Rice Cropping Systems. *Remote Sens,* 14:2770. https://doi.org/10.3390/rs14122770

Saeed, S., Latif, M.A., Rajput, M.A. 2021. Fuzzy-Based Multi-Crop Classification Using High Resolution UAV Imagery. *Quaid-E-Awam University Research Journal of Engineering, Science & Technology, Nawabshah,* 19(1):1-8. https://doi.org/10.52584/QRJ.1901.01

Sivanandam, P., Lucieer, A., 2022. Tree Detection and Species Classification in a Mixed Species Forest Using Unoccupied Aircraft System (UAS) RGB and Multispectral Imagery. *Remote Sens,* 14:4963. https://doi.org/10.3390/rs14194963

Sothe, C., De Almeida, C.M., Schimalski, M.B., et al. 2020. Comparative performance of convolutional neural network, weighted and conventional support vector machine and random forest for classifying tree species using hyperspectral and photogrammetric data. *GIScience & Remote Sensing,* 57:369–394. https://doi.org/10.1080/15481603.2020.1712102

Su, T-H., Wu, C-H., Kao, J-H. 2021. Artificial intelligence in precision medicine in hepatology. *J Gastroenterol Hepatol,* 36:569–580. https://doi.org/10.1111/jgh.15415

Tang, J., Liang, J., Yang, Y., Zhang, S., Hou, H, Zhu, X. 2022. Revealing the Structure and Composition of the Restored Vegetation Cover in Semi-Arid Mine Dumps Based on LiDAR and Hyperspectral Images. *Remote Sens,* 14:978. https://doi.org/10.3390/rs14040978

Tucker, C.J. 1979. Red and photographic infrared linear combinations for monitoring vegetation. *Remote Sens of Environ,* 8(2):127–150. https://doi.org/10.1016/0034-4257(79)90013-0

van Geffen, F., Heim, B., Brieger, F., et al. 2022. SiDroForest: a comprehensive forest inventory of Siberian boreal forest investigations including drone-based point clouds, individually labeled trees, synthetically generated tree crowns, and Sentinel-2

labeled image patches. *Earth Syst Sci Data,* 14:4967–4994. https://doi.org/10.5194/essd-14-4967-2022

Veras, H.F.P., Ferreira, M.P., da Cunha Neto, E.M., et al. 2022. Fusing multi-season UAS images with convolutional neural networks to map tree species in Amazonian forests. *Ecological Informatics,* 71:101815. https://doi.org/10.1016/j.ecoinf.2022.101815

Xu, K., Tian, Q., Zhang, Z., Yue, J., Chang, C-T. 2020. Tree Species (Genera) Identification with GF-1 Time-Series in A Forested Landscape, Northeast China. *Remote Sens,* 12:1554. https://doi.org/10.3390/rs12101554

Xu, Z., Shi, W., Lin, L., et al. 2021. PCA-RF model for Dendrolimus punctatus Walker damage detection. *Nat Hazards,* 106:991–1009. https://doi.org/10.1007/s11069-021-04503-4

Yang, G., Zhao, Y., Li, B., et al. 2019. Tree Species Classification by Employing Multiple Features Acquired from Integrated Sensors. *Journal of Sensors,* 2019:12. https://doi.org/10.1155/2019/3247946

Shi, Y., Skidmore, A.K., Wang, T., et al. 2018. Tree species classification using plant functional traits from LiDAR and hyperspectral data. *International Journal of Applied Earth Observation and Geoinformation,* 73:207-219. https://doi.org/10.1016/j.jag.2018.06.018

Zhong, H., Lin, W., Liu, H., et al. 2022. Identification of tree species based on the fusion of UAV hyperspectral image and LiDAR data in a coniferous and broad-leaved mixed forest in Northeast China. *Front Plant Sci,* 13:964769. https://doi.org/10.3389/fpls.2022.964769

Zhou, G., Ni Z., Zhao, Y., Luan, J. 2022. Identification of Bamboo Species Based on Extreme Gradient Boosting (XGBoost) Using Zhuhai-1 Orbita Hyperspectral Remote Sensing Imagery. *Sensors,* 22:5434. https://doi.org/10.3390/s22145434

Zhou, X.X., Li, Y.Y., Luo, Y.K., et al. 2022. Research on remote sensing classification of fruit trees based on Sentinel-2 multi-temporal imageries. *Sci Rep,* 12:11549. https://doi.org/10.1038/s41598-022154140

Appendix A. The value of the dispersions of the projection of the values of 125 SB attributable to the principal components

2021									
Component	1	2	3	4	5	6	7	8	9
July 02									
Standard deviation	8.404	4.612	3.990	3.229	2.127	1.768	1.427	0.995	-
Proportion of Variance	0.512	0.154	0.115	0.076	0.033	0.023	0.015	0.007	-
Cumulative Proportion	0.512	0.666	0.781	0.857	0.890	0.912	0.927	0.934	-
July 09									
Standard deviation	8.946	4.144	3.965	2.883	2.021	1.633	1.390	0.993	-
Proportion of Variance	0.580	0.124	0.114	0.060	0.030	0.019	0.014	0.007	-
Cumulative Proportion	0.580	0.704	0.818	0.879	0.908	0.927	0.942	0.949	-
July 16									
Standard deviation	8.664	4.316	3.877	3.246	2.053	1.711	1.274	0.988	-
Proportion of Variance	0.544	0.135	0.109	0.076	0.031	0.021	0.012	0.007	-
Cumulative Proportion	0.544	0.679	0.788	0.864	0.895	0.916	0.928	0.935	-
July 23									
Standard deviation	8.952	4.034	3.663	3.318	1.946	1.658	1.126	0.999	-
Proportion of Variance	0.581	0.118	0.097	0.080	0.027	0.020	0.009	0.007	-
Cumulative Proportion	0.581	0.699	0.796	0.876	0.903	0.923	0.932	0.940	-
August 06									
Standard deviation	8.633	4.025	3.852	3.275	2.010	1.802	1.593	1.000	-
Proportion of Variance	0.540	0.117	0.108	0.078	0.029	0.024	0.018	0.007	-
Cumulative Proportion	0.540	0.658	0.765	0.843	0.872	0.896	0.914	0.921	-
August 24									
Standard deviation	8.765	4.356	3.826	3.059	1.914	1.786	1.429	0.991	-
Proportion of Variance	0.557	0.138	0.106	0.068	0.027	0.023	0.015	0.007	-
Cumulative Proportion	0.557	0.694	0.800	0.868	0.895	0.918	0.933	0.940	-
2022									
Component	1	2	3	4	5	6	7	8	9
July 29									
Standard deviation	8.385	4.272	3.273	2.928	2.126	1.644	1.010	0.953	-
Proportion of Variance	0.558	0.145	0.085	0.068	0.036	0.021	0.008	0.007	-
Cumulative Proportion	0.558	0.703	0.788	0.856	0.892	0.913	0.921	0.929	-
August 09									
Standard deviation	8.418	4.338	3.189	2.841	1.837	1.739	0.943	-	-
Proportion of Variance	0.562	0.149	0.081	0.064	0.027	0.024	0.007	-	-
Cumulative Proportion	0.562	0.712	0.792	0.857	0.883	0.907	0.914	-	-

August 15									
Standard deviation	8.607	4.129	3.239	2.888	1.959	1.499	0.967	-	-
Proportion of Variance	0.588	0.135	0.083	0.066	0.030	0.018	0.007	-	-
Cumulative Proportion	0.588	0.723	0.807	0.873	0.903	0.921	0.929	-	-
August 30									
Standard deviation	8.661	4.398	3.290	2.887	1.599	1.445	0.856	-	-
Proportion of Variance	0.595	0.154	0.086	0.066	0.020	0.017	0.006	-	-
Cumulative Proportion	0.595	0.749	0.835	0.901	0.921	0.938	0.944	-	-
September 05									
Standard deviation	8.039	5.184	3.295	3.069	1.692	1.377	1.045	0.790	-
Proportion of Variance	0.513	0.213	0.086	0.075	0.023	0.015	0.009	0.005	-
Cumulative Proportion	0.513	0.726	0.813	0.887	0.910	0.925	0.934	0.939	-
September 12									
Standard deviation	8.667	3.927	3.360	2.898	1.870	1.591	0.861	-	-
Proportion of Variance	0.596	0.122	0.090	0.067	0.028	0.020	0.006	-	-
Cumulative Proportion	0.596	0.719	0.808	0.875	0.903	0.923	0.929	-	-
September 20									
Standard deviation	8.206	4.874	3.213	2.991	1.860	1.498	1.029	0.866	-
Proportion of Variance	0.534	0.189	0.082	0.071	0.027	0.018	0.008	0.006	-
Cumulative Proportion	0.534	0.723	0.805	0.876	0.903	0.921	0.930	0.936	-
September 27									
Standard deviation	8.230	3.981	3.350	3.195	2.040	1.616	1.048	1.032	0.985
Proportion of Variance	0.538	0.126	0.089	0.081	0.033	0.021	0.009	0.008	0.008
Cumulative Proportion	0.538	0.663	0.753	0.834	0.867	0.887	0.896	0.904	0.912
October 03									
Standard deviation	7.936	4.540	3.343	3.147	2.234	1.693	1.091	1.040	0.947
Proportion of Variance	0.500	0.164	0.089	0.079	0.040	0.023	0.009	0.009	0.007
Cumulative Proportion	0.500	0.663	0.752	0.831	0.870	0.893	0.903	0.911	0.918
October 10									
Standard deviation	8.937	3.877	3.342	2.737	1.745	1.374	0.818	-	-
Proportion of Variance	0.634	0.119	0.089	0.059	0.024	0.015	0.005	-	-
Cumulative Proportion	0.634	0.753	0.842	0.901	0.926	0.941	0.946	-	-
October 17									
Standard deviation	8.612	4.361	3.418	2.969	1.786	1.385	0.849	-	-
Proportion of Variance	0.589	0.151	0.093	0.070	0.025	0.015	0.006	-	-
Cumulative Proportion	0.589	0.740	0.832	0.902	0.928	0.943	0.949	-	-
October 24									
Standard deviation	8.560	3.723	3.574	2.888	1.940	1.488	1.029	0.986	-
Proportion of Variance	0.582	0.110	0.101	0.066	0.030	0.018	0.008	0.008	-
Cumulative Proportion	0.582	0.692	0.793	0.860	0.889	0.907	0.915	0.923	-